ARTICLE

Response Surface Methodology and Deep Learning Modelling for the Removal of Pb^{2+} ions from Wastewater Using Apple Pomace

Great C. Chazuza [1]* ⓘ , *Felicia O. Afolabi* [1] ⓘ , *Paul Musonge* [2] ⓘ

[1] *Chemical Engineering Department, Durban University of Technology, Steve Biko Campus, 151 Steve Biko Rd, Durban, Kwazulu Natal 4001, South Africa*

[2] *Faculty of Engineering, Mangosuthu University of Technology, 511 Griffiths Mxenge Hwy, Umlazi, Durban, Kwazulu Natal 4031, South Africa*

ABSTRACT

Recent studies have demonstrated a growing global interest in utilising agricultural waste to remediate wastewater. This stems from growing apprehensions about high levels of heavy metals, especially Pb^{2+} ions, in wastewater produced by industrial processes such as mining, paint production, oil refining, smelting, and electroplating. This study examined apple pomace's Pb^{2+} ions adsorption from wastewater. Response Surface Methodology (RSM) was employed, utilising the central composite face-centred design (CCFD) with three variables: initial concentration (1–50 mg/L), adsorbent dosage (0.1–1 g), and particle size (75–425 μm) to formulate a mathematical model for the biosorption of Pb^{2+} ions on apple pomace. An artificial neural network (ANN) was developed using data generated from the RSM design. The CCFD and ANN models showed considerable efficacy in the adsorption process, exhibiting correlation coefficient values of 0.9921 and 0.9999, respectively. The isotherm and kinetic studies were performed, and the Freundlich Isotherm model best fitted the equilibrium data, with a correlation coefficient of 0.972 and a q$_e$ of 5.145 mg/g. Additionally, the pseudo-second-order model proved to be the most appropriate for the kinetic data, with an R^2 of 0.9996. These results confirm that apple pomace functions as an effective, low-cost, and environmentally and sustainably biosorbent for the removal of Pb^{2+} ions from wastewater. Both RSM and ANN models exhibited high predictive capability for the biosorption process. While ANN

*CORRESPONDING AUTHOR:

Great C. Chazuza, Chemical Engineering Department, Durban University of Technology, Steve Biko Campus, 151 Steve Biko Rd, Durban, Kwazulu Natal 4001, South Africa; Email: 22288261@dut4life.ac.za

provides more flexibility in modelling complex non-linear relationships, it is prone to overfitting, particularly with limited datasets, and this was addressed through a 5-fold cross-validation technique.

Keywords: Wastewater; Potable Water; Biosorption; Apple Pomace; Response Surface Methodology; Deep Learning Modelling; ANN

1. Introduction

The global demand for clean water continues to escalate due to population growth, driving the expansion of industrial and domestic activities, alongside rapid urbanisation to accommodate rising human settlements[1,2]. These changes complicate the management of a consistent supply of clean water due to the increased production of wastewater laden with contaminants, particularly heavy metals from industrial effluents and other anthropogenic sources[2–7]. In nearly all major industrial sectors, it is unavoidable to circumvent lead-containing compounds during processing. Hence, Pb^{2+} ions are among the most prevalent heavy metals in industrial effluents, with the mining, battery, paint, oil refining and smelting industries being the major contributors to their discharge[8,9]. Lead ions have high solubility in aquatic organisms such as fish, and are easily absorbed through their skin and soft tissues. Once absorbed, they enter the food chains, ultimately affecting human health upon consumption. The lead ions interact vigorously with proteins and other macromolecules, thereby deactivating them and causing potential accumulation of Pb^{2+} ions in certain organs, which can result in chronic poisoning. Some of the negative impacts caused by lead ions include Alzheimer's disease, damage to renal and reproductive systems and other nervous system disorders[10,11].

The Environmental Protection Agency (EPA) and the World Health Organization (WHO) set stringent maximum permissible concentrations for heavy metals in drinking water and wastewater to safeguard both human and environmental health. For Pb^{2+} ions, the EPA limit is 0.015 mg/L, while the WHO guideline is even more conservative at 0.01 mg/L[8,12]. These guidelines incorporate not only the environmental concerns but also the toxicological limits beyond which lead can trigger neurological, renal, and developmental disorders in humans. These benchmarks serve as critical performance targets for water treatment technologies. In the context of this research, these limits by the WHO and the EPA were used as benchmark criteria for the evaluation of the effectiveness of apple pomace as a biosorbent. Reducing Pb^{2+} ion concentrations below these benchmarks is imperative for any treatment technology to be deemed viable for practical and regulatory compliance.

Furthermore, Pb^{2+} ions may also infiltrate groundwater and natural water bodies via geogenic processes, such as leaching, and can also be present in antiquated lead water pipes, particularly in older cities, due to pipe deterioration. This presents a substantial threat to the quality standards of potable water, since it may become polluted by the time it reaches the end user's tap, despite appropriate treatment at the treatment plants.

To solve this water crisis, researchers worldwide are exploring biosorption as a cost-effective solution to remove heavy metals in wastewater due to its eco-friendliness, flexibility of design, and high efficiency. It is a phenomenon in which ions or molecules from an aqueous solution bind to the biomass by diverse methods, contingent upon the structure and functional groups of the biosorbent[10,13,14]. Furthermore, biosorption has a high capability of occurring across a broad temperature spectrum, pressure and pH, and there is a high probability of the recovery of the adsorbates for reuse in other applications[10,15,16]. Presently, sanctioned biosorption mechanisms include surface complexing, ion exchange, electrostatic action, enzymatic mechanism, redox mechanism, and inorganic precipitation.

Apple pomace is among the most underutilised biosorbents with significant potential. It is a lignocellulosic solid residue generated during the mechanical extraction of juice from apples. This by-product is generated during the pressing stage of juice and cider manufacturing. It primarily consists of peels, pulp, seeds, and stems, and accounts for approximately 25–35% of the original fruit mass, depending on the cultivar variety of apple and the processing conditions. Due to its high moisture content, rapid perishability, and very low commercial value, apple pomace is often discarded or used as low-value animal feed[17,18]. Annually, 12 million tons of

apple pomace are generated worldwide, and the quantity is anticipated to continue increasing due to the ever-expanding global population [17,19]. Functional groups present in apple pomace include –COO (carboxylate), –CO (carbonyl), –NH$_2$ (amino), –OH (hydroxyl), among others, and these are responsible for binding heavy metals [19]. Utilising apple pomace as a biosorbent aligns with circular economy principles by converting waste into a valuable resource for water treatment.

This study aims to evaluate the performance of apple pomace as a biosorbent for Pb^{2+} ion removal from aqueous media. The research focuses on both experimental characterisation and predictive modelling using RSM and ANNs. The study began with the preparation and characterisation of the biosorbent pre- and post-adsorption using the Fourier transform infrared spectroscopy (FTIR) to determine the functional groups present on the biosorbent surface, scanning electron microscopy (SEM) to determine the surface structure of the biosorbent, and energy dispersive X-ray (EDX) for elemental analysis. The second objective was to model the experimental data by employing RSM and ANN modelling. RSM is a statistical approach utilised for experimental design and optimisation of process variable effects, and it was founded on the principles of design of experiments (DOE). It is employed to determine if a set of factors affects the response and if they interact. It also helps to formulate and optimise response behaviour as a function of independent factors, while deep learning within machine learning uses layered neural networks to predict complex data patterns, usually from huge datasets. ANN modelling is a deep learning approach that serves as an intelligent system capable of predicting output patterns by recognising input patterns. ANNs employ a mathematical framework to analyse information and solve complex problems using concepts inspired by a biological brain model [20,21]. The RSM model provides a direct assessment of variable interactions, and from a computational standpoint, RSM is lightweight and easy to implement, especially when dealing with a limited number of variables and experimental runs. It requires solving a set of regression equations, which is less resource-intensive and more transparent, rendering it advantageous for preliminary process evaluation. RSM, while potentially less flexible in modelling complex behaviours,

is often more stable under small input variations. In contrast, ANN functions as a black-box model that is superior in handling intricate, non-linear systems, including subtle variations, which may be overlooked by RSM's polynomial structure [22]. While ANN is powerful in capturing deep patterns in large, high-dimensional datasets, it may suffer from overfitting and lower interpretability. ANN demands more computational power and training time, particularly when working with larger datasets or using more complex network architectures. However, with modern computing resources, this cost is often manageable.

Isotherm and kinetic studies for Pb^{2+} ions removal using apple pomace were also conducted to evaluate the biosorbent capacity and adsorption rate, respectively. The adsorption isotherms at a fixed temperature delineate the correlation that exists between the concentrations of the adsorbate and the degree of its adsorption on the adsorbent surface at equilibrium. The kinetic experiments offer essential insights into the possible mechanisms of biosorption and elucidate the rate at which sorbate adheres to the surface of the biosorbent. Numerous kinetic models have been documented in the literature; however, those focused on the order of reactions, namely the Pseudo-first-order (PFO) and the Pseudo-second-order (PSO) models, are of significant interest [12].

2. Materials and Methods

2.1. Preparation of Adsorbent

Apple pomace used as an adsorbent was sourced from Elgin Fruit Juices (Pty) Ltd, situated in Cape Town, South Africa. It was initially collected in a wet state from the plant and dried at 110 °C for 24 hr at the company. Prior to application, it was re-dried at 60 °C to eliminate any moisture that may have accumulated during transportation and storage. Afterwards, it was ground into powder using a laboratory grinder (Retsch GmbH 5657 HAAN WEST-GERMANY). Afterwards, it was sieved into particles of different sized particles of sizes, ranging from 75 µm to 425 µm. FT-IR (Cary 630, Agilent, USA), SEM-EDX (Zeiss Ultra Plus FEG SEM (Germany); with the Oxford X-Max EDX detector (UK)) were then used to analyse the biosorbent before and post adsorption.

2.2. Preparation of Adsorbate Stock Solution

A stock solution of 500 mg/L of Pb^{2+} ions was generated through dissolving 0.799 g of lead (II) nitrate $[Pb(NO_3)_2]$ in 1000 mL of deionised water in a volumetric flask, followed by meticulous agitation to guarantee the full dissolution of all lead nitrate. Deionised water was used to ensure the absence of competing ions in the solution.

2.3. Response Surface Methodology

To conduct RSM, the DOE was employed using Design Expert 13 software under the central composite face-centred design (CCFD) with three variables at 3 different levels namely −1, 0, and +1, and with 6 central points, yielding 20 experimental runs. The CCFD was selected for its efficiency in exploring quadratic response surfaces and ability to estimate second-order models without requiring a full three-level factorial experiment. This design has high efficiency in capturing non-linear curvature, providing rotatability, and ensuring uniform precision in prediction across the experimental domain, thereby enhancing the reliability of optimisation results. The investigated parameters comprised the initial concentration (A), adsorbent dosage (B), and particle size (C). These variables, along with their respective domains, were chosen based on preliminary batch experiments and were aligned with ranges that are regularly reported in the literature for biosorption studies [8,22]. This safeguarded the relevance and feasibility of the selected experimental domain. Experimental independent variables and their coded levels are outlined in **Table 1**. The experiment produced a single response, the Pb^{2+} ions removal efficiency (%). Analysis of variance (ANOVA) was implemented to determine the correlation between the inputs and responses, as well as the significance of the regression model.

Table 1. Experimental variables and their coded levels (CCFD).

Factor	Variable	Units	Coded Low	Mean	Coded High
			−1	0	1
A	Initial Concentration	mg/l	1.00	25.50	50.00
B	Adsorbent Dosage	g	0.10	0.55	1.00
C	Particle Size	μm	75.00	250.0	425.00*

Note: *Due to the unavailability of sieve plates with a 250 μm mesh size, a 300 μm mesh size was used instead.

Removal Efficiency

The Pb^{2+} ions removal percentage (%) and biosorption capacity of the biosorbent (q) were calculated using Equations (1) and (2).

$$\text{Percentage removal (\%)} = \frac{C_i - C_f}{C_i} \times 100 \qquad (1)$$

$$\text{Biosorption capacity (q)} = \frac{(C_i - C_f) \cdot V}{m} \qquad (2)$$

Where C_i represents initial adsorbate concentration (mg/L), C_f denotes the final adsorbate concentration (mg/L), V signifies the volume of the solution (L), while m represents the biosorbent mass (g).

2.4. ANN Modelling

ANN was developed in MATLAB R2024b using the dataset generated from the RSM matrix based on central composite design (CCFD) and its corresponding experimental responses, to predict removal efficiency. The ANN model was implemented using a feed-forward backpropagation neural network consisting of three input nodes in the input layer, initial concentration, particle size, and adsorbent dose, along with a hidden layer consisting of six neurons that utilise a tangent sigmoid transfer function and a single output node, demonstrating the removal efficiency [4,23]. The architecture of the ANN employed is shown in **Figure 1**.

RSM-derived synthetic dataset consisted of 100 observations with a desirability of 1, each characterised by the three input variables and a corresponding removal efficiency. Prior to training, all the input and output variables were normalised using min-max scaling to the (0,1) range, to ensure consistent scaling across all features and facilitate faster convergence during training. The partitioning of the data into training, testing, and validation sets was conducted randomly into 70% training data, 15% validation data and 15% testing data. This typical partitioning ensured that the model training and evaluation were conducted on mutually

exclusive subsets. Model training was performed using the Levenberg–Marquardt optimisation algorithm, which is well-suited for small- to medium-sized datasets and provides fast convergence. Model training was performed over a maximum of 1000 epochs. To reduce overfitting and improve generalisation, early stopping was implemented based on validation performance. No supplementary regularisation techniques were employed; the default mean squared error (MSE) function and correlation coefficients (R^2) served as the performance metrics for the single split evaluation.
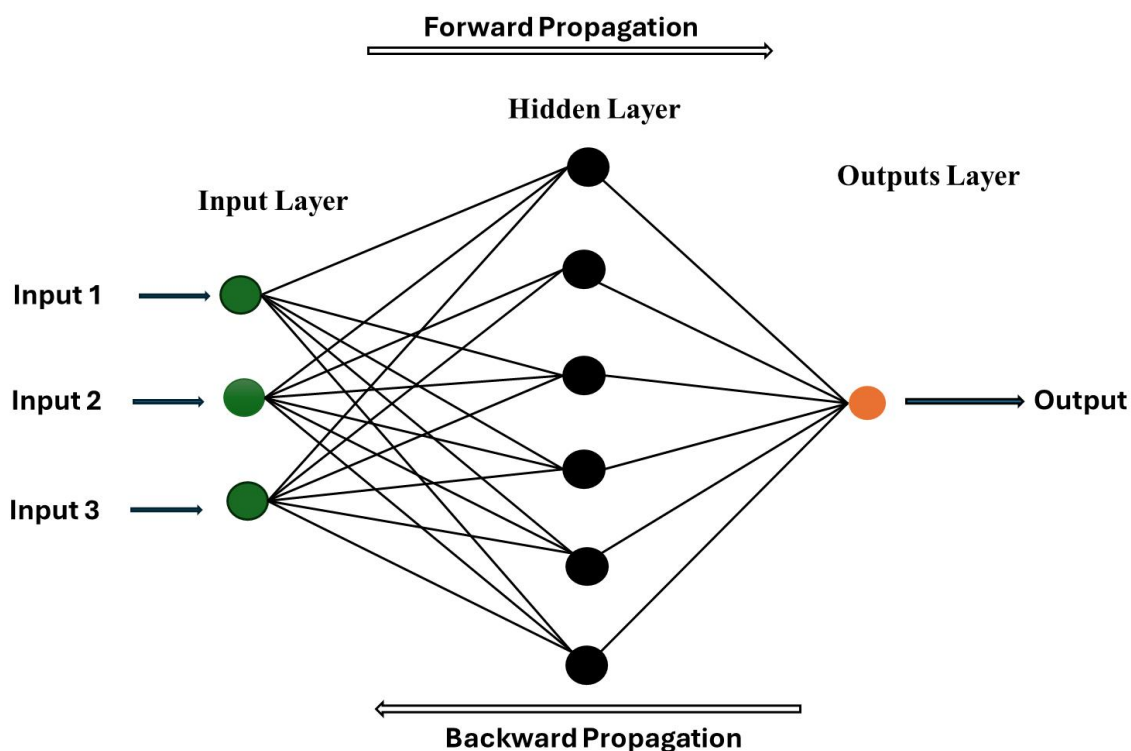

Figure 1. Structure of ANN.

Given the relatively small dataset size, which can be a limiting factor in deep learning applications, the k-fold cross-validation technique was employed to provide a more robust estimate of model performance. This technique helps reduce the variance associated with a single train-test split and provides a more conservative and reliable assessment of the ANN's generalisation capacity.

While other models, such as Random Forests, offer strong predictive power, effectively handle nonlinearities, and provide feature importance metrics, they balance between interpretability and performance. ANN stands out for its customizable architectures and its ability to capture deeper patterns in large, high-dimensional datasets tailored to specific problems [24]. Meanwhile, RSM, beyond its interpretability, provides explicit equations and clear insights into variable effects and interactions, making it well-suited for process optimisation [22].

2.5. Isotherm Study

A series of $Pb(NO_3)_2$ solutions with a range of concentrations between 5 and 50 mg/L was generated from a stock solution by serial dilutions. Each 100 mL aliquot was transferred into a labelled conical flask. Afterwards, the pH of each solution was measured with a pH meter (SensoDirect 150), and adjusted to 5.5 to prevent precipitation of Pb as Lead hydroxide [$Pb(OH)_2$], which will exaggerate the removal efficiency and conceal the true adsorption behaviour. This was followed by the loading of 0.55 g of adsorbent (150 μm particle size) to each flask. The mixtures were consistently agitated on a linear shaker (Model 262, Trilab Support, CC, South Africa) at 180 rpm for 120 minutes at room temperature (25 ± 1 °C) to ensure equilibrium was attained. After agitation, the solutions were filtered using Whatman filter paper, followed by 0.45 μm pore-sized syringe filters. The

spent adsorbent residues were dried in a standard oven (Scientific 221) at 60 °C until a constant weight was attained. The residues were then characterised using FT-IR, SEM, and EDX methods. The filtrates were analysed with a micro-plasma atomic emission spectrophotometer (MY 18379001, Agilent, USA) to measure the remaining Pb^{2+} ions post-adsorption. All the experiments were carried out in duplicates, and the mean values were used to enhance the reliability of the results. The Langmuir and the Freundlich isotherm models were employed to model the experimental data.

The Langmuir isotherm model is represented by the following Equation (3).

$$Q_e = \frac{Q_{max}bC_e}{1 + bC_e} \qquad (3)$$

The terms in the above equation represent the following: Q_{max} is the maximum adsorption capacity of the metal ion in mg/g, while b represents the Langmuir constant (L/mg); q_e denotes the adsorption capacity at equilibrium (mg/g); and Ce represents the final adsorbate concentration at equilibrium (mg/L).

The Freundlich model is presented by Equation (4).

$$q_e = K_f C_e^{\frac{1}{n}} \qquad (4)$$

The terms of the equation above signify the following, K_f and n are constants, while q_e represents the equilibrium adsorption capacity (mg/g), and C_e denotes the final adsorbate concentration at equilibrium (mg/L).

The Langmuir isotherm model assumes that the adsorbent's surface is homogeneous and smooth, with minimal lateral interactions among adsorbed molecules. It also presumes uniform adsorption energy across all adsorption sites, irrespective of the substances adsorbed in adjacent sites[25]. In contrast, the Freundlich isotherm model assumes that the adsorbent's surface is heterogeneous, comprising various adsorption sites with differing affinities for the adsorbate. This model accommodates multilayer adsorption, where multiple layers of adsorbate molecules may develop on the adsorbent's surface[25]. It also suggests that adsorption capacity increases continuously with concentration, implying a theoretically unlimited adsorption capacity. Furthermore, it also assumes that the adsorption energy fluctuates across the surface of the adsorbent, leading to a nonlinear adsorption behaviour.

2.6. Kinetic Study

To investigate the adsorption kinetics of Pb^{2+} ions, 50 mg/L lead nitrate solutions were prepared by precise serial dilutions of the stock solution. These solutions were transferred into two separate 1000 mL beakers, labelled A and B, to facilitate parallel experimentation. The beakers were placed on a jar test apparatus (VELP JLT6), a device commonly used for controlled mixing in water treatment studies. Afterwards, 2 g of adsorbent was added to each beaker and the solutions were agitated at 180 rpm for 24 hours at ambient temperature. We employed sampling intervals of 5, 10, 15, 20, 30, 45, 60, 90, 120, 150, 180, 240, 300, and 360 minutes, with the final samples taken at 24 hours. This interval spacing afforded adequate precision to fully document the swift initial adsorption and the eventual attainment of the equilibrium.

The experiments were conducted in duplicate to ensure the reproducibility of the results. The PFO and PSO kinetic models were used to validate the authenticity of the kinetic data. Both models assume that the sorption rate is directly proportional to the quantity of available active sites on the biosorbent surface, following either a first or second order rate relationship[14]. However, the two models differ in their assumptions concerning the adsorption mechanism. PFO is generally associated with physisorption, while PSO is for chemisorption as the rate-limiting step[26].

Pseudo-first-order reaction:

$$\ln(q_e - q_t) = \ln q_e - k_1 t \qquad (5)$$

Pseudo-Second-Order reaction:

$$\frac{t}{q_t} = \frac{1}{k_2 q_e^2} + \frac{t}{q_e} \qquad (6)$$

In the above equations, q_e stands for the amount of adsorbate (mg/g) adsorbed at equilibrium, while q_t corresponds to the quantity of adsorbate adsorbed at a specific time (t). t stands for time (h), k_1 for the PFO reaction rate constant (h), and k_2 for the PSO reaction rate constant (g mg^{-1} h^{-1}). We choose the best model based on the numerical value of the coefficient of determination.

3. Results and Discussion

3.1. FT-IR Spectroscopy Analysis

The FTIR spectra of apple pomace powder were analysed before and after Pb^{2+} ion adsorption (**Figure 2**), within the wavenumber range of 398 to 4000 cm^{-1} and a resolution of 4 cm^{-1}, to determine the adsorbent's functional groups using FT-IR (Cary 630, Agilent, USA). The FT-IR spectrum prior to adsorption exhibited multiple significant peaks, indicating the presence of active functional groups on the biosorbent surface. The peaks observed in the range of 3000 to 3600 cm^{-1} and around 1000 cm^{-1} correspond to –OH stretching vibrations. A peak between 2800 and 3000 cm^{-1} was attributed to C–H stretching in aliphatic chains, while the region between 1400 and 1700 cm^{-1} was associated with –C=O, NH and C=C groups. After adsorption, noticeable shifts and changes in transmittance intensity were observed in these regions, indicating interactions between metal ions and the surface functional groups. Upward shifts in peak positions and spectral changes suggest that the identified functional groups actively participated in the binding of Pb^{2+} ions. The existence of negatively charged functional groups like the hydroxyl and carboxylic groups led to the conclusion that the adsorption of Pb^{2+} ions occurred primarily through electrostatic attraction. The adsorption mechanism likely involves ion exchange, whereby Pb^{2+} ions substitute other native cations (Ca^{2+}, K^+, or H^+) present on the surface of the adsorbent. Additionally, hydrogen bonding and Van der Waals forces may contribute to Pb^{2+} ions retention due to the involvement of oxygen- and hydrogen-containing groups.
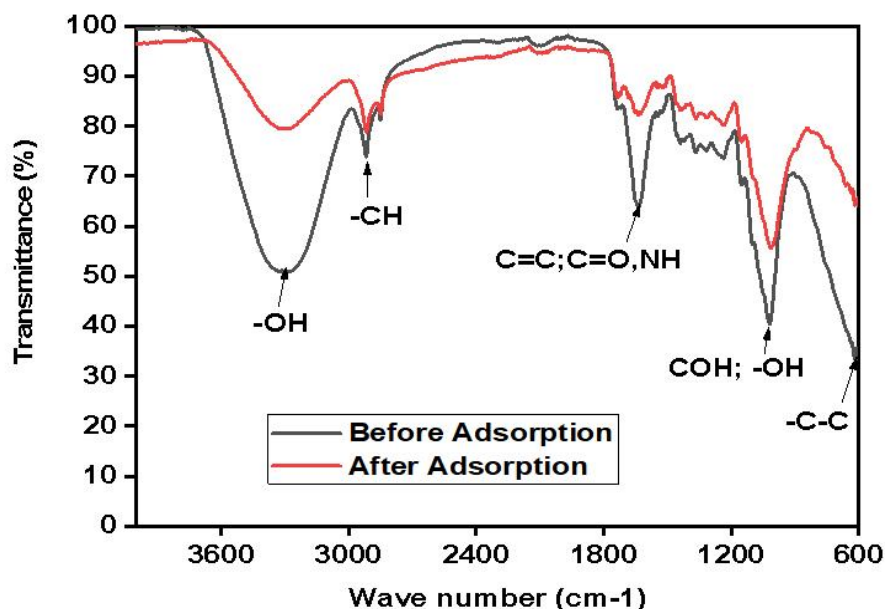

Figure 2. FT-IR spectra (before and after adsorption).

3.2. SEM-EDX Analysis

Surface morphology analysis of apple pomace was performed using Zeiss Ultra Plus FEG SEM (Germany). The samples were mounted on aluminium SEM stubs using adhesive carbon tape, and subsequently gold sputter-coated with the Quorum Q 150 RES sputter coater (UK) to enhance conductivity prior to imaging. SEM images were captured at a working distance of 8.9 mm and a magnification of 5,000x at an accelerating voltage of 20 kV, to provide detailed insights into the porous and uneven surface topology of the apple pomace. EDX was performed simultaneously with SEM for elemental mapping, using an Oxford X-Max EDX detector (UK).

SEM-EDX analysis showed how the surface morphology of the adsorbent material appeared before and after Pb^{2+} ion adsorption. When scanned under the SEM, the initial adsorbent surface featured large irregularities, as shown in **Figure 3a**. The uneven surface promotes heavy metal adsorption through deposition and stronger ion-bonding of Pb^{2+} ions at those uneven points. A substantial surface morpholog-

ical modifications of the adsorbent were observed through the SEM image in **Figure 3b** after Pb^{2+} ions were adsorbed. The surface developed a flatter texture because Pb^{2+} ions settled tightly into biosorbent pores and obstructed the holes. The Pb^{2+} ion show chemical bonding through carboxylic and hydroxyl surface functional sites of the adsorbent. The surface transformation patterns that occurred during Pb^{2+} ions adsorption revealed that our adsorbent material successfully captured heavy metals from solution. The study reveals how the material's surface structures participate in assessing the possible occurrence of adsorption and the effectiveness of the adsorbent in removing Pb^{2+} ions from wastewater.


(a)   (b)
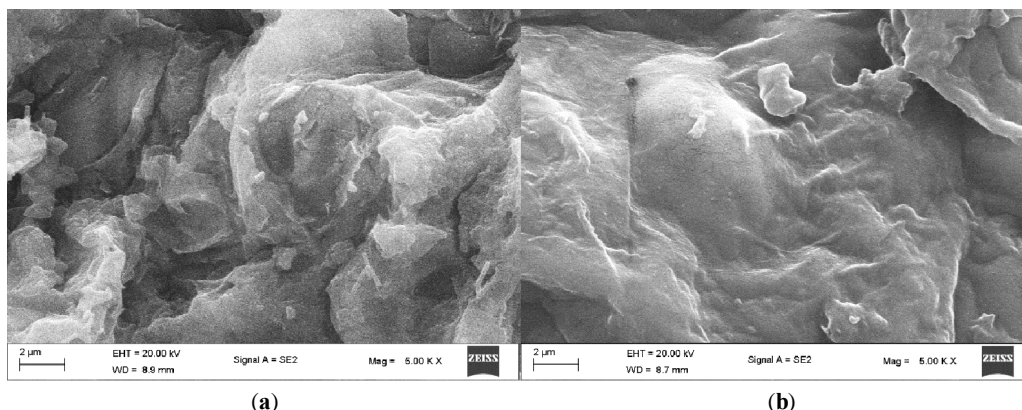
Figure 3. SEM analysis of AP: (**a**) Before adsorption; and (**b**) After adsorption.

3.3. EDX Analysis

Figure 4 shows the spectra of apple pomace before and after Pb^{2+} ion adsorption. EDX analysis of the raw apple pomace, shown in **Figure 4a**, indicates that it contains carbon (63.89 wt%) and oxygen (35.73 wt%). It also has trace amounts of calcium (0.07 wt%) and potassium (0.30 wt%) as shown in **Table 2**. These findings indicate that apple pomace can be useful as an adsorbent material, with its surface chemistry being the pivot of adsorption. During the adsorption process, Pb^{2+} ions were deposited on the biosorbent surface, resulting in significant alterations in elemental composition. The decrease in carbon content and increased oxygen levels proved that apple pomace reacted with Pb^{2+} ions through its carboxylic and hydroxyl groups. The biosorbent surface showed evidence of ion exchange as potassium disappeared after adsorption, as shown in **Figure 4b**.

(a)
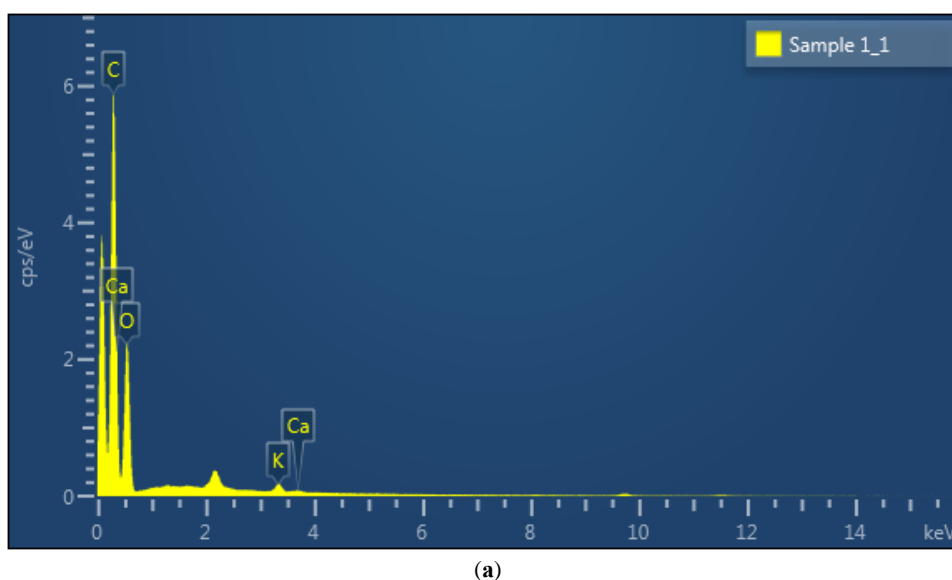
Figure 4. *Cont.*
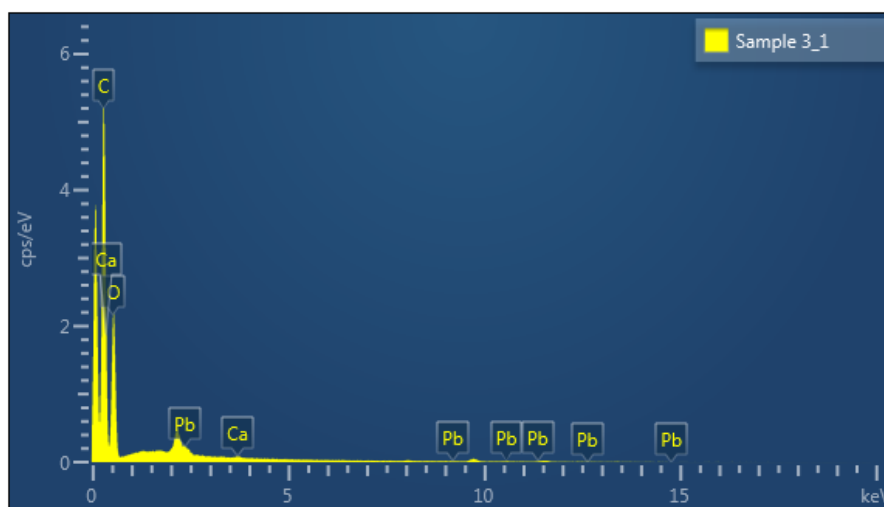
(**b**)

Figure 4. EDX spectra of AP: (**a**) Before Pb^{2+} ions adsorption; and (**b**) After Pb^{2+} ions adsorption.

Table 2. Percentage composition of elements in apple pomace.

Element	C	O	K	Ca	Pb
Wt % before adsorption	63.89	35.73	0.30	0.07	0
Wt % after adsorption	59.53	39.75	0	0.07	0.65

3.4. RSM Modelling

The RSM was analysed using Design-Expert 13 software. **Table 3** presents the design matrix, which includes the independent variables, actual experimental responses, and predicted outcomes.

A quadratic model [Equation (7)] was formulated to describe the removal efficiency of Pb^{2+} ions from wastewater. This model was presented using coded factors based on the independent variables A, B and C. It is validity and statistical significance were evaluated using ANOVA, which confirmed its capacity to predict the adsorption process.

Table 3. RSM experimental design matrix with responses.

Std.	Run	Factor 1 A: Initial Concentration mg/l	Factor 2 B: Adsorbent Dosage g	Factor 3 C: Particle Size um	Response Removal % Experimental	Response Removal% Predicted
6	1	50	0.1	425	29	29.43
18	2	25.5	0.55	250	78.94	80.11
9	3	1	0.55	250	88,00	87.88
13	4	25.5	0.55	75	89.21	88.7
15	5	25.5	0.55	250	78.94	80.11
17	6	25.5	0.55	250	78.94	80.11
16	7	25.5	0.55	250	78.94	80.11
2	8	50	0.1	75	54.09	55.07
12	9	25.5	1	250	77.53	79.04
14	10	25.5	0.55	425	73.37	72.92
1	11	1	0.1	75	77.65	77.92
4	12	50	1	75	68.97	68.43
20	13	25.5	0.55	250	84.01	80.11
3	14	1	1	75	90.38	90.18
11	15	25.5	0.1	250	63.1	60.64
10	16	50	0.55	250	62.15	61.31
19	17	25.5	0.55	250	79,00	80.11
8	18	50	1	425	54,00	53.97
5	19	1	0.1	425	60.05	60.83
7	20	1	1	425	85.01	84.27

$$(Y) = 80.11 - 13.29A + 9.2B - 7.89C + 0.27AB$$
$$- 2.14AC + 2.79BC - 5.52A^2 - 10.28B^2 \quad (7)$$

The model's overall performance was assessed by analysing the magnitude of its regression coefficient of determination R^2 (0.9921), adjusted R^2 (0.9850) and the predicted R^2 (0.9703). All the coefficients of the regression models were close to 1, signifying a strong positive correlation and a strong fit between the model's predicted and experimental data. A low coefficient of variance (1.85%) indicated low variability between predicted values and actual values, as presented in **Table 4**.

Table 4. Model fit statistics.

Parameter	Value	Parameter	Value
Std. Dev.	1.85	R^2	0.9921
Mean	72.56	Adjusted R^2	0.9850
C.V. %	2.55	Predicted R^2	0.9703
		Adeq Precision	46.4795

The predicted R^2 (0.9703) is in strong agreement with the Adjusted R^2 (0.9850), showing a discrepancy of less than 0.2.

3.4.1. ANOVA Results

ANOVA results showed that the developed model has high statistical significance, with an F-value of 139.55, indicating a 0.01% chance that this high value could result from random variation. p-values less than 0.05 represented the significant terms of the model, and in this analysis, terms A, B, C, AC, BC, A² and B² were identified as significant contributors to the model's predictive ability. Moreover, the F-value of 0.60 for lack of fit suggests that the lack of fit is not statistically significant relative to the pure error, reinforcing the adequacy of model fit. These F-values and p-values, summarised in **Table 5**, confirm the model's effectiveness in modelling the relationship between variables and responses. **Figure 5** illustrates that the predicted values closely correspond with the actual values, further indicating a high degree of model accuracy and minimal error.

Table 5. Analysis of variance (ANOVA) of the model for the removal of Pb^{2+} ions.

Source	Sum of Squares	df	Mean Square	F-Value	p-Value	
Model	4,291.00	9	476.78	139.55	< 0.0001	**Significant**
A-Initial Concentration	1,765.71	1	1765.71	516.80	< 0.0001	
B-Adsorbent Dosage	846.40	1	846.40	247.73	< 0.0001	
C-Particle Size	622.05	1	622.05	182.06	< 0.0001	
AB	0.5995	1	0.5995	0.1755	0.6842	
AC	36.51	1	36.51	10.69	0.0084	
BC	62.44	1	62.44	18.28	0.0016	
A²	83.75	1	83.75	24.51	0.0006	
B²	290.54	1	290.54	85.04	< 0.0001	
C²	1.33	1	1.33	0.3903	0.5461	
Residual	34.17	10	3.42			
Lack of Fit	12.84	5	2.57	0.6024	0.7042	**not significant**
Pure Error	21.32	5	4.26			
Cor Total	4,325.17	19				

3.4.2. 3D Surface Plots

Figure 6 aids in comprehending the influence of independent variables and their interactions on the dependent variable. The interactive effects of adsorbent dosage and particle size are illustrated in the three-dimensional surface plot representing factor BC in **Figure 6a**. The initial concentration of Pb^{2+} ions is consistently maintained at 25 mg/L. The removal efficiency increased gradually as the dosage increased and the size of the adsorbent particles decreased. This phenomenon can be ascribed to the increased availability of surface area and the increasing ratio of adsorbent to Pb^{2+} ion concentration, which increases the number of active sites. The percentage of removal, however, begins to

decrease as the dosage increases. This is due to agglomeration, which reduces the amount of surface area available and the total number of active sites for metal adsorption by obscuring some active sites on the adsorbent surface.
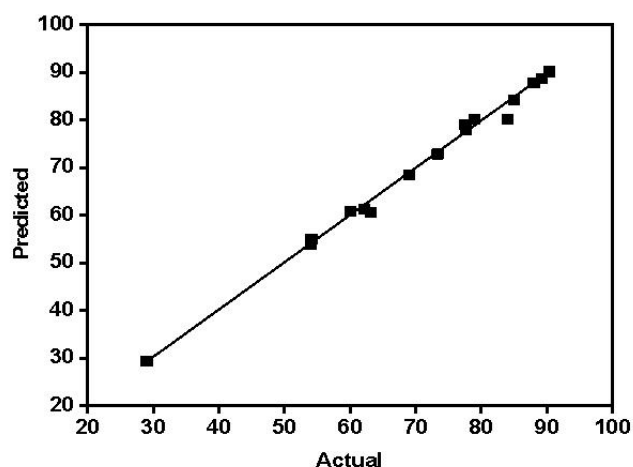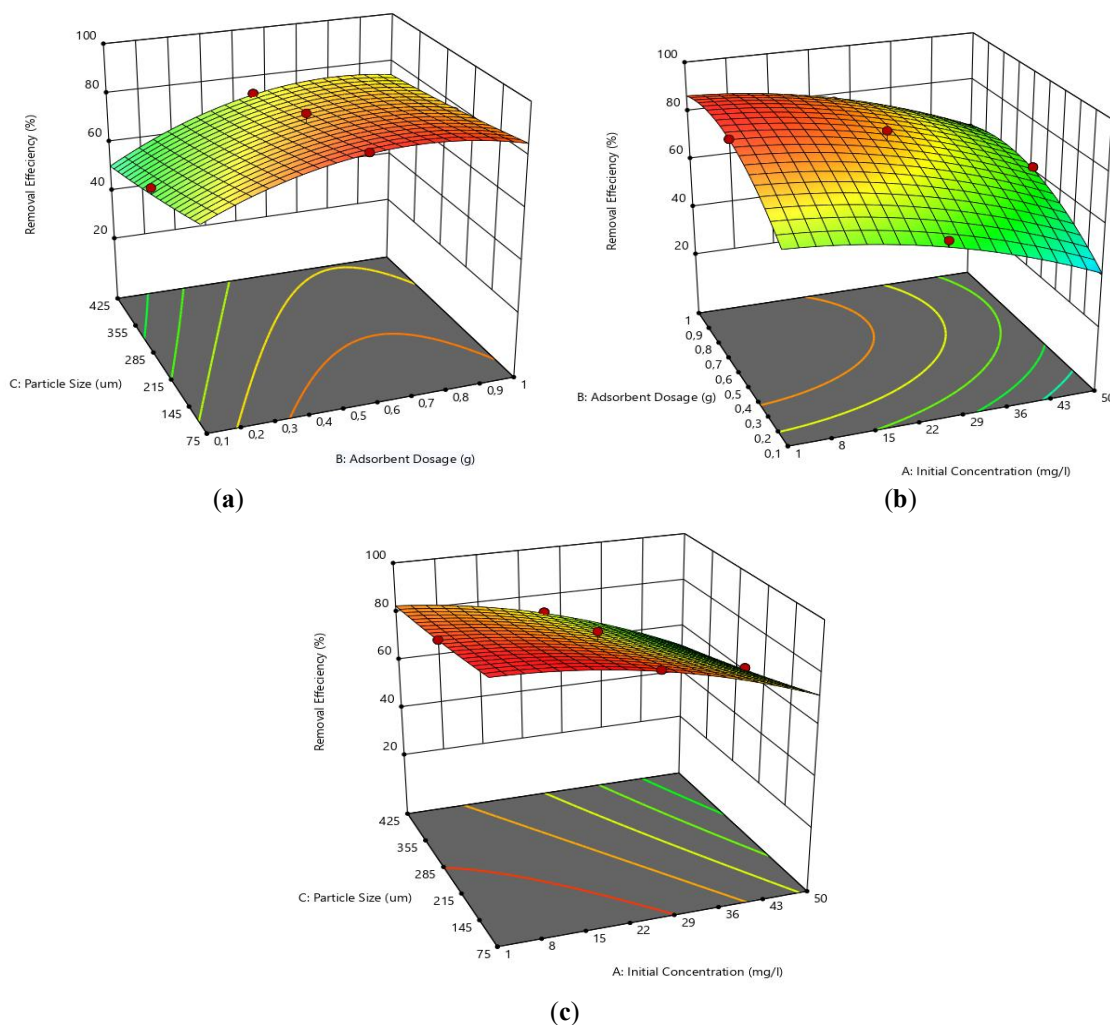

Figure 5. Predicted vs. actual plot.

(**a**)

(**b**)

(**c**)

Figure 6. 3D Surface plots: (**a**) Effect of particle size and dosage on removal efficiency of Pb^{2+} ions; (**b**) Effect of initial concentration and adsorbent dosage on removal efficiency of Pb^{2+} ions; and (**c**) Effect of particle size and initial concentration on removal efficiency of Pb^{2+} ions.

In **Figure 6b**, at a fixed particle size (C) of 250 μm, the 3D surface plot shows that a rise in the initial concentration coupled with a decrease in dosage results in a decrease in the percentage of removal. This is due to the reduced surface area and due to the reduced number of particles in the solution. Removal efficiency increases as the adsorbent dosage is increased because more particles present an enhanced surface area. The most favourable percentage removal occurs at lower initial metal ion concentrations with a high dosage of adsorbent (1 g). In the surface plot in **Figure 6c**, we observe that at fixed adsorbent dosage, the increase in the initial concentration of Pb^{2+} ions and particle size of the biosorbent leads to the decline of the removal percentage of the Pb^{2+} ions. This is because the larger the particle size, the smaller the surface area, and hence the fewer active sites for metal adsorption from the solution to occur. Higher removal is obtained at lower initial concentration and smaller particle size due to increased surface area to solute concentration ratio.

3.4.3. Optimization

The evaluation of the most effective conditions for removing Pb^{2+} ions was performed to determine the factors that removing removal efficiency. The optimal parameters identified for the maximum removal of Pb^{2+} ions included an initial concentration of 15.08 mg/L, an adsorbent dosage of 0.789 g, and a particle size of 98.82 μm, resulting in a removal efficiency of 91.95%, along with a desirability factor of 1. The analysis of observed trends and implemented optimisations indicates that the efficacy of apple pomace in removing Pb^{2+} ions is enhanced at lower concentrations. Specifically, at concentrations below 20 mg/L, apple pomace can eliminate nearly 90% of Pb^{2+} ions from the aqueous solution. The optimisations constraints considered are shown in **Table 6**.

Table 6. Optimisations constraints.

Name	Goal	Lower Limit	Upper Limit	Lower Weight	Upper Weight	Importance
A: Initial Concentration	is in range	1	50	1	1	4
B: Adsorbent Dosage	is in range	0.1	1	1	1	3
C: Particle Size	is in range	75	425	1	1	3
Removal Efficiency	maximize	29	90.38	1	1	5

3.5. ANN Modelling Results

3.5.1. Regression Plots

Figure 7 displays four regression plots that show the relationship of output to target values across training and validation sets, test sets and the full dataset. The regression line, along with the correlation coefficient (R-values), indicates the degree of alignment between the network's predictions and the actual target values. The model is highly effective in learning the features of the training data, as evidenced by its R-value of 0.9999, indicating a strong correlation. The system has a high capacity to successfully extend to new data because its validation set yields an exceptionally strong correlation of 0.9999. The test data sets show a high R-value of 0.9999, which proves a strong performance level. The combined R-value measurement of 0.9999 supports the notion that our neural network can successfully predict the correlation between input variables and output values in every data arrangement. Model training results are summarised in **Table 7**.

Table 7. Model training results on single-split performance.

	Observations	MSE	R	R^2
Training	70	0.0024	0.9999	0.9999
Validation	15	0.0065	0.9999	0.9999
Test	15	0.0031	0.9999	0.9999

The histogram in **Figure 8** shows how neural network outputs compare to target values and displays the accuracy of each dataset type. The blue, green, and red bars in the histogram display the training, validation, and test datasets, respectively. The number of errors indicates excellent network performance, as most errors appear close to the zero-error line. A symmetrical distribution centred around this line suggests a well-balanced model.
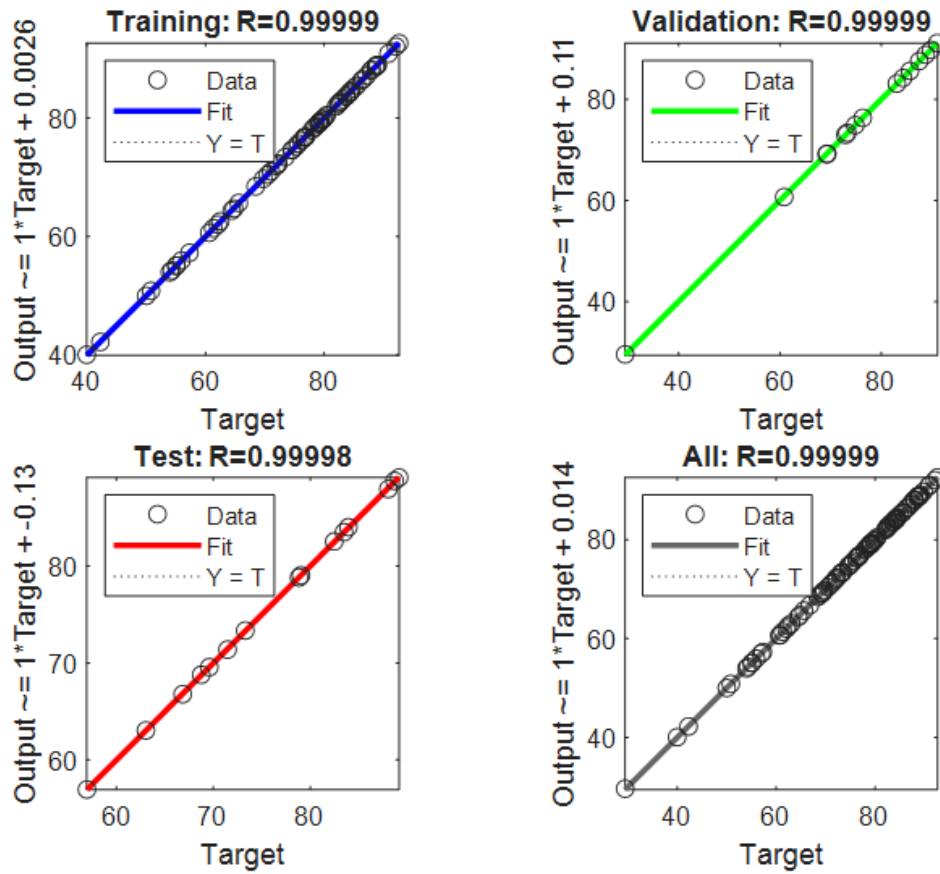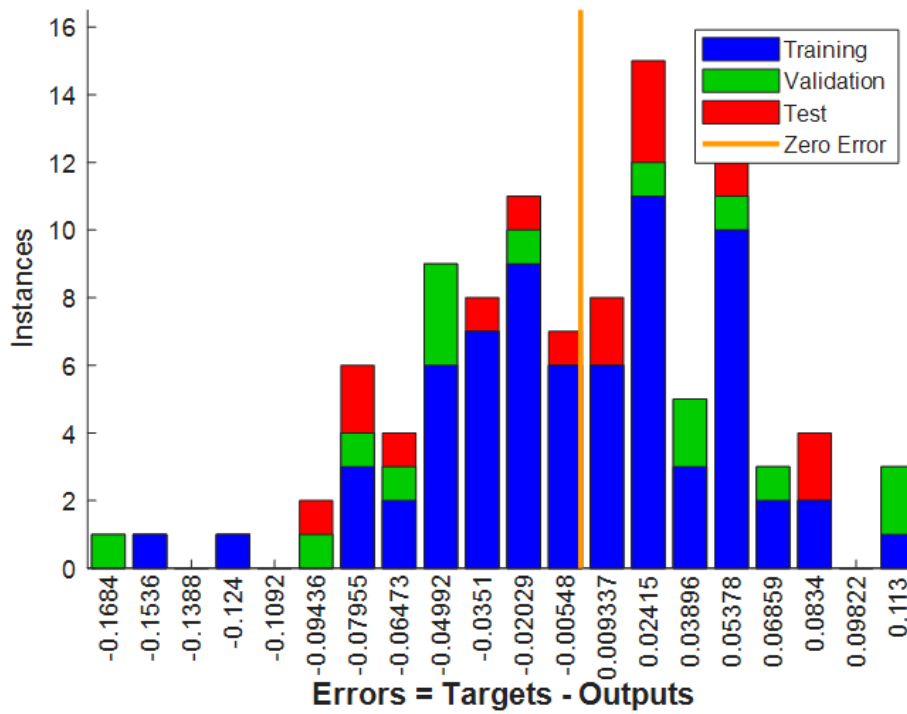
Figure 7. Model regression plots.

Figure 8. Error histogram.

The network system shows great prediction accuracy, with the majority of errors falling within the range of −0.05 to 0.05, indicating close proximity to zero error. All the errors, training, validation and test errors are well distributed around the zero error line, indicating good generalisation capability and minimal overfitting.

3.5.2. Performance Plot

Figure 9 shows the performance plot of MSE for the training, validation, and test datasets over 182 epochs. The point of optimal validation performance is highlighted at epoch 176. The MSE drops markedly in the early epochs, indicating rapid learning by the network, with convergence observed around epoch 100. At epoch 176, the validation error reaches its lowest value (0.0064742), after which no significant improvements were observed. The test error closely follows the validation error, which supports the model's ability to generalise well to unseen data. Furthermore, the low and stable MSE observed across all data subsets shows effective training and minimal signs of overfitting.
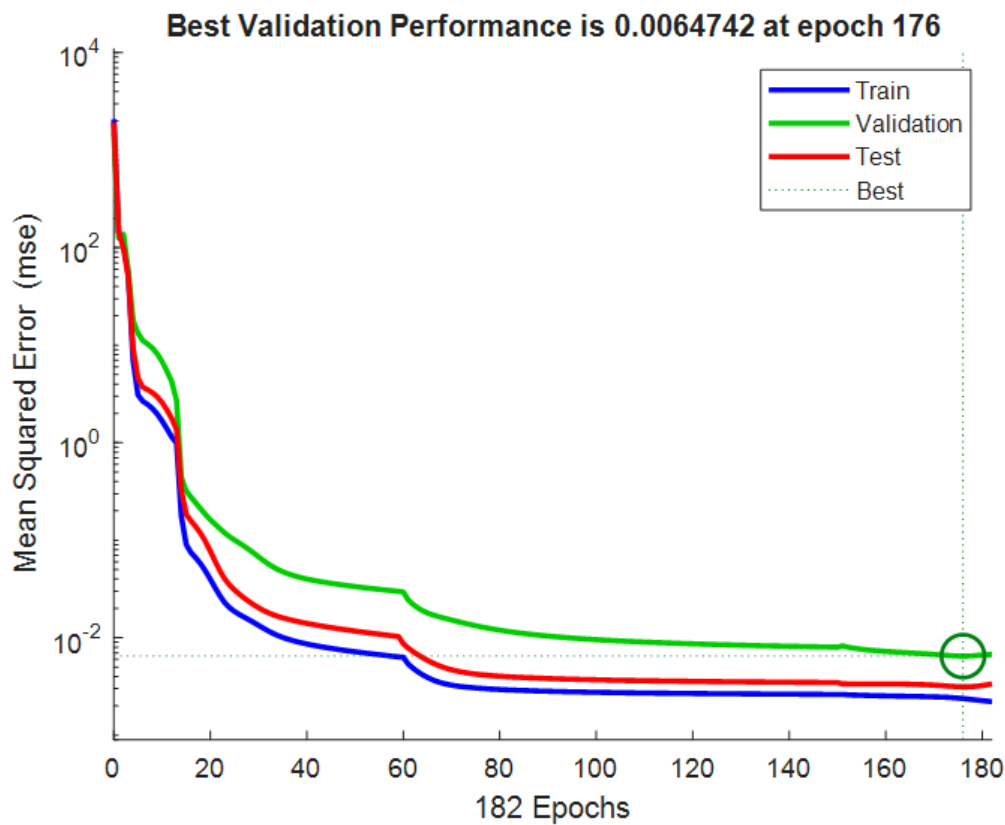

**Figure 9.** Model performance plot.

3.6. K-Fold Cross-Validation

K-fold cross-validation was employed by splitting the dataset into five equal segments (5-fold cross-validation), where the model was trained on four segments and validated on the remaining one, rotating through all combinations. The technique confirmed the model's generality, as reflected in the consistent performance across all folds, as evidenced by the average training RMSE of 0.0311, average validation RMSE of 0.1743, average validation R^2 of 0.9996, and average validation MSE of 0.0385. **Figures 10–12** present the fold-wise MSE, RMSE and R^2 values, respectively. The relatively lower average error metrics indicate enhanced predictive accuracy. However, the noticeable increase in validation error in fold 5 indicates variability in model generalisation, which may warrant further examination. This could be attributed to underlying data characteristics within that subset, such as distribution shifts or the presence of influential data points.
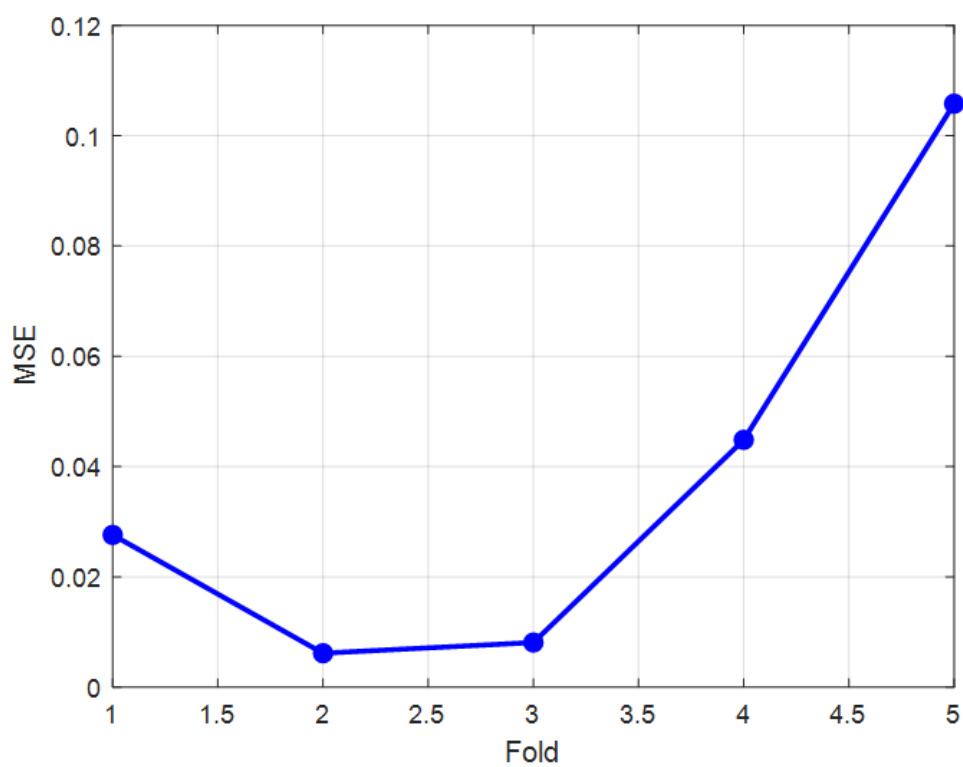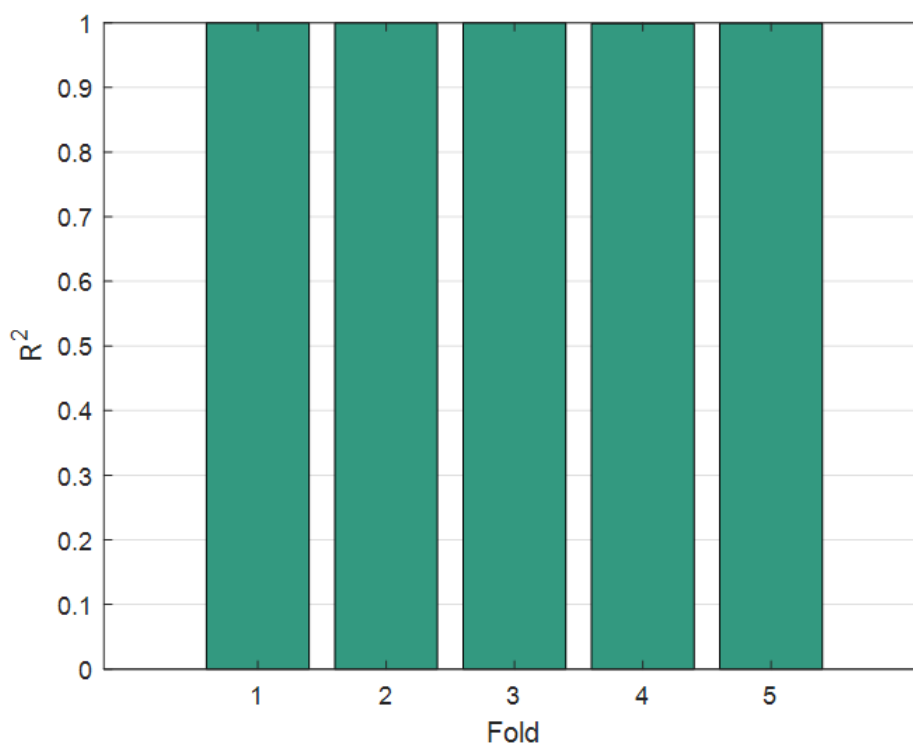
Figure 10. 5-fold cross-validation (MSE per fold).
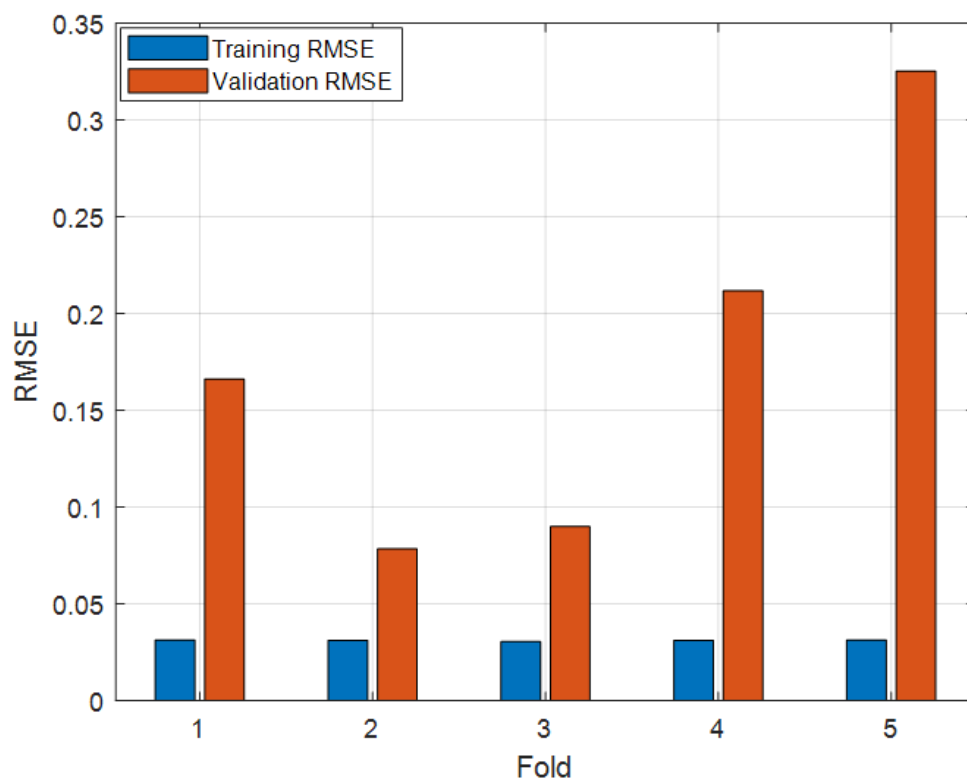
**Figure 11.** 5-fold cross-validation (RMSE per fold).

Figure 12. 5-fold cross-validation (R^2 per fold).

Figure 13a–e shows the validation results from all folds, illustrating direct comparison between predicted and actual Pb^{2+} ion removal efficiencies. These predicted values closely align with the true experimental values, with very minimal deviation throughout all five datasets. This strong alignment reinforces the model's high predictive capability, indicating that the developed ANN model effectively captures all the underlying nonlinear relationships within the experimental data. The removal efficiency values ranged from nearly 29% to 91.50 %; thus, the model was able to accurately predict both low and high removal scenarios. These results validate the robustness and dependability of the ANN model for simulating the biosorption of Pb^{2+} ions utilising apple pomace as a biosorbent.
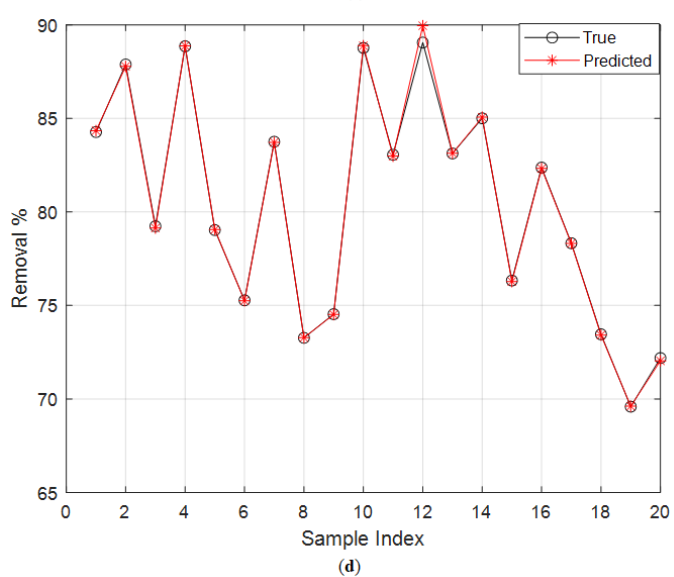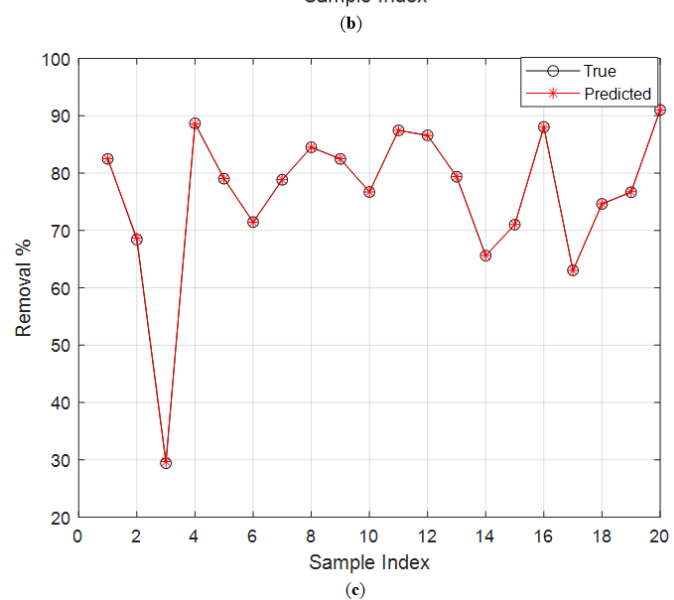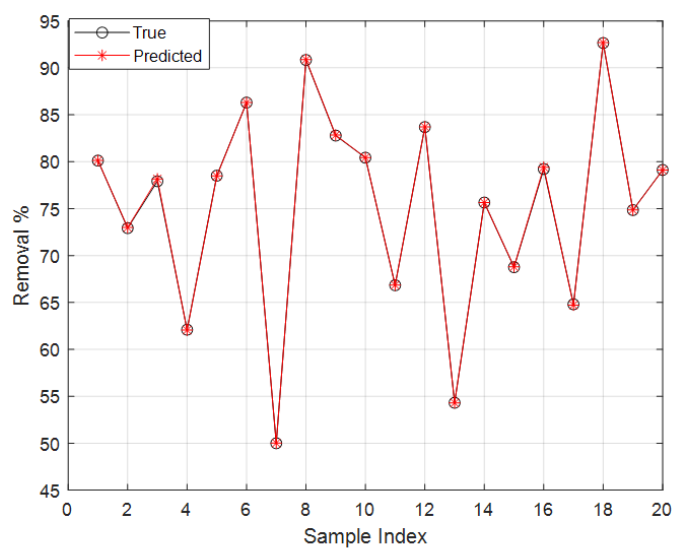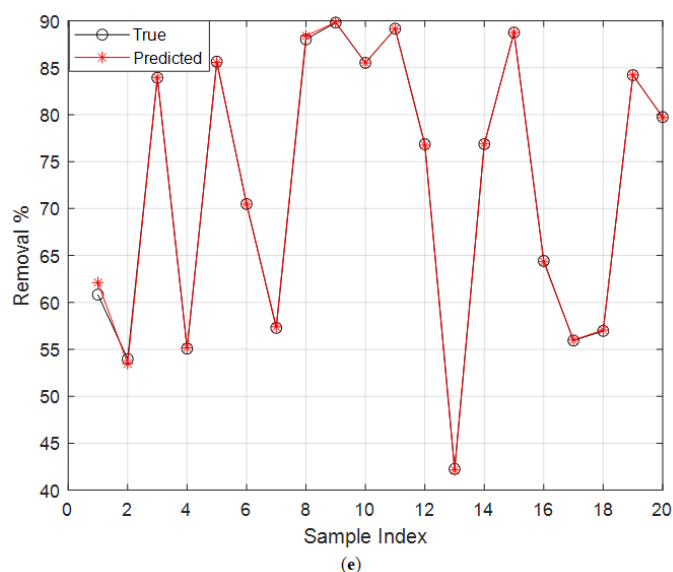

(a)

Figure 13. *Cont.*

(b)


(c)

(d)
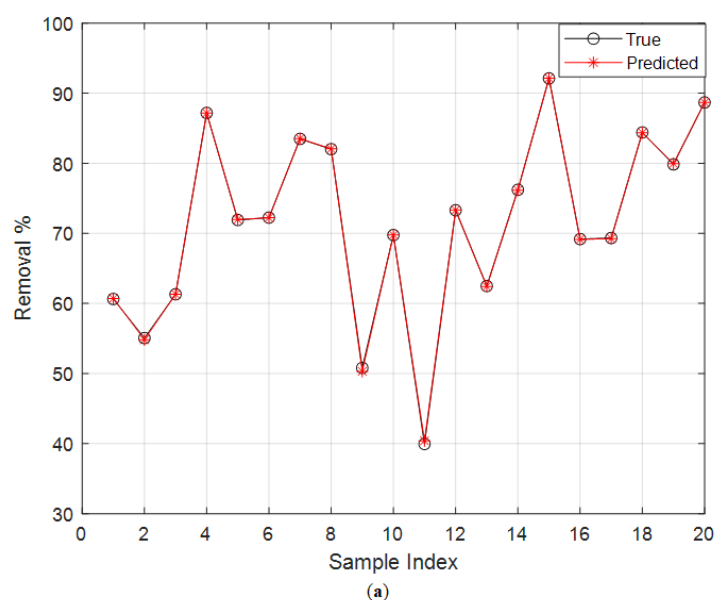
Figure 13. *Cont.*

Figure 13. True vs predicted validation output: (**a**) Fold 1-validation output; (**b**) Fold 2-validation output; (**c**) Fold 3-validation output; (**d**) Fold 4-validation output; and (**e**) Fold 5-validation output.

While deep learning models generally require larger datasets, the feed-forward ANN employed in this study exhibited sufficient flexibility in modelling non-linear relationships between the parameters, resulting in commendable prediction accuracy.
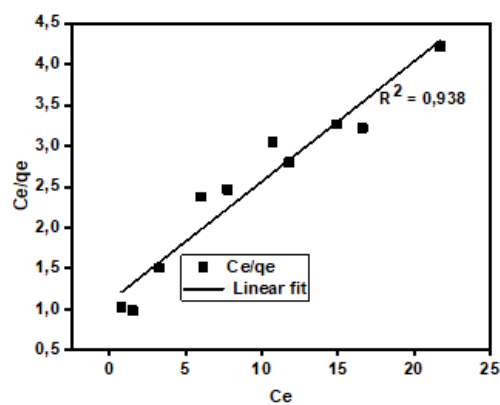
3.7. Adsorption Isotherms

To validate the adsorption data, two isotherm models were applied, the Freundlich model and the Langmuir model (**Figure 14**). As shown in **Figure 14a**, the Freundlich isotherm presented an excellent fit for the adsorption data, with a higher correlation ($R^2 = 0.973$) and an estimated ad-

sorption capacity ($q_e = 5{,}145$ mg/g), compared to the Langmuir model with R^2 (0.938) (**Figure 14b**). This superior fit suggests heterogeneous surface adsorption and the potential for multilayer formation, as assumed by the Freundlich isotherm model. This aligns with the inherent structural complexity of apple pomace, which contains diverse functional groups unevenly distributed across the biosorbent surface. These groups offer multiple binding sites with varying affinities, which deviates from the monolayer, uniform surface assumption of the Langmuir model. Moreover, the computed value of n (greater than 1) shown in **Table 6** indicates exceptional adsorption.
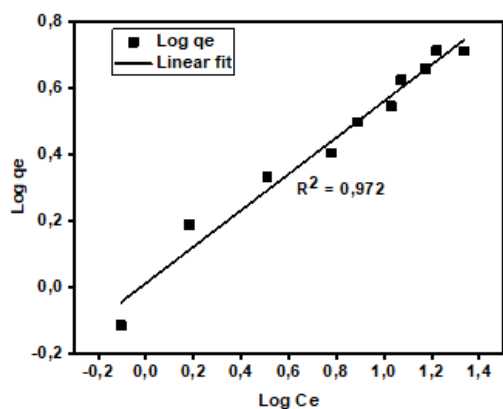
Figure 14. Isotherm models: (**a**) Freundlich; and (**b**) Langmuir.

Although the Freundlich model showed a better fit, it indicates multilayer adsorption on a heterogeneous surface. However, the Langmuir model still provided a useful theoretical estimate of monolayer adsorption maximum adsorption capacity (Q_{max} = 6.80 mg/g), representing monolayer coverage. This suggests the surface approaches saturation at higher Pb^{2+} concentrations. Therefore, integrating insights from both models along with the consideration of biosorbent uneven structure provides a more comprehensive understanding of the adsorption behaviour, suggesting the coexistence of both multilayer and monolayer mechanisms, which reflects surface heterogeneity and saturation limits.

Furthermore, the adsorption capacity increased with rising initial adsorbate concentration, from 0.77 mg/g at 5 mg/L to a maximum of 5.145 mg/g at 50 mg/L. This performance is significantly higher than that reported by Gryko et al. (2021), who achieved a maximum of 0.248 mg/g using raw apple pomace. The variations can be attributed to several factors, including differences in initial concentrations used (50 mg/L in this study vs. 10 mg/L in theirs), pre-treatment methods, and contact time (90 minutes in their study). Their apple pomace may have had a different phytochemical profile due to cultivar or processing conditions.

The observed increase in adsorption capacity with Pb^{2+} ion concentration corresponded to an increase in the driving force for mass transfer[27]. At lower concentrations, adsorption increases almost linearly, as sufficient active sites are available. However, as the concentration approaches higher values, the rate of increase in adsorption capacity diminishes, suggesting that the surface is approaching saturation.

Although the linearised models employed here allow efficient estimation of the constants and comparative evaluation of biosorption performance between models, they do not accurately depict saturation plateaus at elevated concentrations, but these models remain widely accepted for modelling adsorption at moderate concentrations. Overall, the results highlight the strong adsorption potential of apple pomace and confirm the adsorption capacities consistent with those reported in the literature. **Table 8** summarises the parameters obtained from all isotherm models evaluated.

Table 8. Isotherm model parameters.

Model	Parameter	Value	Units
Langmuir model $Q_e = \frac{Q_{max}bC_e}{1+bC_e}$	Q_{max}	6.80	mg/g
	b	0.13	L/mg
	R^2	0.938	None
Freundlich model	R^2	0.972	None
	q_e	5.145	mg/g
	K_f	1.01176	L/g
	n	1.821	None

3.8. Adsorption Kinetics

The kinetic experimental data were examined by fitting them to both PFO and PSO models (**Table 9**). The PFO model had a relatively small negative correlation, as demonstrated by a weak correlation coefficient of R^2 = 0.263 (**Figure 15a**), but the PSO model revealed an excellent relationship, with a coefficient of R^2 = 0.999 (**Figure 15b**). The PSO model indicates that the adsorption process is affected by the numbe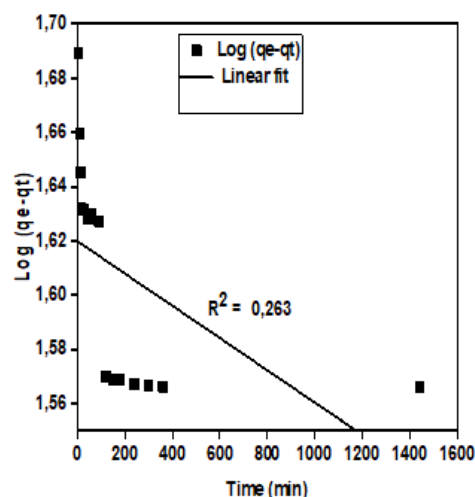r of active sites on the adsorbent's surface, with the adsorption rate directly proportional to the square of the available vacant sites. This indicates that the adsorption of Pb^{2+} ions onto apple pomace is primarily governed by chemisorption rather than Van der Waals forces or other molecular interactions. This implies that the rate-limiting step likely involves valence forces through the sharing or exchange of electrons between the metal ions and the functional groups on the apple pomace. This mechanism is consistent with literature reports for biosorbents rich in lignocellulosic material and functional groups[25,28].
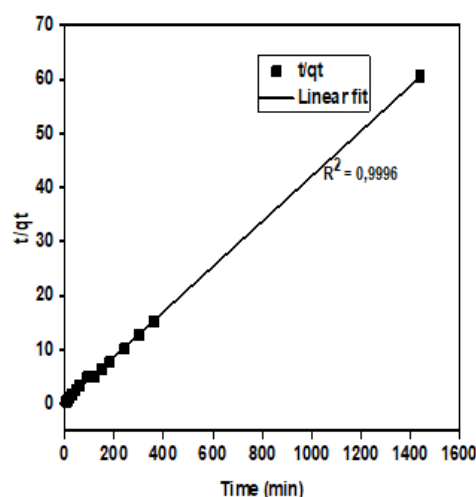
Table 9. Kinetic models' parameters.

Model	Parameter	Value	Units
PFO model	q_e	5.053	mg/g
$\ln(q_e - q_t) = \ln q_e - k_1 t$	k_1	6×10^{-5}	min^{-1}
$y = 1.62 - 0.00006t$	R^2	0.263	None

Table 9. *Cont.*

Model	Parameter	Value	Units
PSO model $\frac{t}{q_t} = \frac{1}{k_2 q_e^2} + \frac{t}{q_e}$ $y = 0.0417x - 0.3586$	q_e k_2 R^2	23.98 0.00453 0.9996	mg/g g/mg None

Figure 15. Kinetic models: (**a**) PFO model; and (**b**) PSO model.

4. Conclusion

Apple pomace demonstrated significant potential as an economical and sustainable biosorbent for the removal of Pb^{2+} ions from both potable and wastewater, with removal efficiency influenced by the initial metal ion concentration. The adsorption data were effectively modelled using the established RSM quadratic model, exhibiting a standard deviation of 1.85 and a strong correlation ($R^2 = 0.9921$). The optimal parameters for Pb^{2+} ion adsorption identified were an initial concentration of 15.08 mg/L, a dose of 0.789 g, and a particle size of 98.98 μm, resulting in a removal efficiency of 91.95%. All input variables significantly influenced adsorption efficiency, as revealed through interaction effect analysis.

Additionally, an ANN model was successfully developed based on the RSM experimental design matrix, achieving an overall correlation of $R^2 = 0.9999$ in a single split evaluation and an average R^2 exceeding 0.9999 across five-fold cross-validation, alongside an MSE of 0.0385, indicating the model's robustness across all data subsets. While ANN provided slightly superior predictive accuracy, RSM offered better interpretability and experimental optimisation capability.

The Freundlich isotherm ($R^2 = 0.98$) best described the adsorption process, indicating multilayer adsorption on the heterogeneous surface. This is consistent with the complex organic composition and irregular morphology of apple pomace[29]. The adsorption kinetics followed the PSO model, suggesting chemisorption as the rate-limiting step, involving electron-sharing or covalent bonding between Pb^{2+} ions and surface functional groups such as –COOH and -OH, as supported by FTIR analysis.

Overall, the findings strongly support the viability of utilising apple pomace as a low-cost biosorbent for the removal of Pb^{2+} ions in batch-scale treatment systems. Apple pomace is generated in significant quantities annually and is often disposed of at minimal cost. Nevertheless, the study's scope is limited to batch-scale experiments. To better evaluate real-world applicability and scalability, future studies should investigate fixed-bed column systems, dynamic adsorption behaviour, and the impact of multi-component wastewater matrices under realistic operating conditions.

Author Contributions

Methodology, G.C.C.; investigation, G.C.C.; resources, F.O.A.; data curation, G.C.C.; writing—original draft preparation, G.C.C.; writing—review and editing, F.O.A.; supervision, F.O.A. and P.M.; project administration, P.M.; funding acquisition, P.M. All authors have read and agreed to the published version of the manuscript.

Funding

Institutional Review Board Statement

Not applicable.

Informed Consent Statement

Not applicable.

Data Availability Statement

Data will be provided upon request.

Acknowledgments

Conflicts of Interest

The authors declare that there is no conflict of interest.

References

[1] van Vliet, M.T.H., Jones, E.R., Flörke, M., et al., 2021. Global Water Scarcity Including Surface Water Quality and Expansions of Clean Water Technologies. Environmental Research Letters. 16, 024020. DOI: https://doi.org/10.1088/1748-9326/abbfc3

[2] Tekin, B., Acikel, U., 2023. Adsorption Isotherms for Removal of Heavy Metal Ions (Copper and Nickel) From Aqueous Solutions in Single and Binary Adsorption Processes. Gazi University Journal of Science. 36(2), 495–509. DOI: https://doi.org/10.35378/gujs.1066137

[3] Shrestha, R., Ban, S., Devkota, S., et al., 2021. Technological Trends in Heavy Metals Removal From Industrial Wastewater: A Review. Journal of Environmental Chemical Engineering. 9(4), 105688. DOI: https://doi.org/10.1016/j.jece.2021.105688

[4] Yildiz, S., 2018. Artificial Neural Network Approach for Modeling of Ni(II) Adsorption From Aqueous Solution by Peanut Shell. Ecological Chemistry and Engineering S. 25(4), 581–604. DOI: https://doi.org/10.1515/eces-2018-0039

[5] Bayuo, J., Rwiza, M.J., Sillanpaa, M., et al., 2023. Removal of Heavy Metals From Binary and Multicomponent Adsorption Systems Using Various Adsorbents – A Systematic Review. RSC Advances. 13(19), 13052–13093. DOI: https://doi.org/10.1039/d3ra01660a

[6] Chen, F., Zhao, Y., Zhao, H., et al., 2024. Heavy Metal Removal From Wastewater Using Poly(Gamma-Glutamic Acid)-Based Hydrogel. Gels. 10(4), 259. DOI: https://doi.org/10.3390/gels10040259

[7] Dagne, B.B., 2020. Determination of Heavy Metals in Wastewater and Their Toxicological Implications Around Eastern Industrial Zone, Central Ethiopia. Journal of Environmental Chemistry and Ecotoxicology. 12(2), 72–79. DOI: https://doi.org/10.5897/jece2019.0453

[8] Afolabi, F.O., Musonge, P., Bakare, B.F., 2021. Application of the Response Surface Methodology in the Removal of Cu2+ and Pb^{2+} From Aqueous Solutions Using Orange Peels. Scientific African. 13, e00931. DOI: https://doi.org/10.1016/j.sciaf.2021.e00931

[9] Agoro, M.A., Adeniji, A.O., Adefisoye, M.A., et al., 2020. Heavy Metals in Wastewater and Sewage Sludge From Selected Municipal Treatment Plants in Eastern Cape Province, South Africa. Water. 12(10), 2746. DOI: https://doi.org/10.3390/w12102746

[10] Thirunavukkarasu, A., Nithya, R., Sivashankar, R., 2021. Continuous Fixed-Bed Biosorption Process: A Review. Chemical Engineering Journal Advances. 8, 100188. DOI: https://doi.org/10.1016/j.ceja.2021.100188

[11] Singh, N., Yadav, A., Das, S., et al., 2024. Recent Ad-

vances in Heavy Metal/Metalloid Ion Treatment From Wastewater Using Nanocomposites and Bionanocomposites. Frontiers in Nanotechnology. 6, 1307353. DOI: https://doi.org/10.3389/fnano.2024.1307353

[12] Khan, T., Ul Mustafa, M.R., Isa, M.H., et al., 2017. Artificial Neural Network (ANN) for Modelling Adsorption of Lead (Pb (II)) From Aqueous Solution. Water, Air, & Soil Pollution. 228, 426. DOI: https://doi.org/10.1007/s11270-017-3613-0

[13] Huang, D., Li, B., Ou, J., et al., 2020. Megamerger of Biosorbents and Catalytic Technologies for the Removal of Heavy Metals From Wastewater: Preparation, Final Disposal, Mechanism and Influencing Factors. Journal of Environmental Management. 261, 109879. DOI: https://doi.org/10.1016/j.jenvman.2019.109879

[14] Michalak, I., Chojnacka, K., Witek-Krowiak, A., 2013. State of the Art for the Biosorption Process – A Review. Applied Biochemistry and Biotechnology. 170, 1389–1416. DOI: https://doi.org/10.1007/s12010-013-0269-0

[15] Poonam, Rani, A., Sharma, P.K., 2021. Biosorption: Principles, and Applications. In: Gupta, L.M., Ray, M.R., Labhasetwar, P.K. (eds.). Advances in Civil Engineering and Infrastructure Development. Springer: Singapore. pp. 501–510.

[16] Acheampong, M.A., Meulepas, R.J.W., Lens, P.N.L., 2010. Removal of Heavy Metals and Cyanide From Gold Mine Wastewater. Journal of Chemical Technology & Biotechnology. 85(5), 590–613. DOI: https://doi.org/10.1002/jctb.2358

[17] Ungureanu, G., Enache, I.M., Cara, I.G., et al., 2024. Insights Into the Environmental Benefits of Using Apple Pomace for Biosorption of Lead From Contaminated Water. Heliyon. 10(17), e36811. DOI: https://doi.org/10.1016/j.heliyon.2024.e36811

[18] Gryko, K., Kalinowska, M., Świderski, G., 2021. The Use of Apple Pomace in Removing Heavy Metals From Water and Sewage. Environmental Sciences Proceedings. 9(1), 24. DOI: https://doi.org/10.3390/environsciproc2021009024

[19] Chand, P., Pakade, Y.B., 2013. Removal of Pb From Water by Adsorption on Apple Pomace: Equilibrium, Kinetics, and Thermodynamics Studies. Journal of Chemistry. 2013(1), 164575. DOI: https://doi.org/10.1155/2013/164575

[20] Nighojkar, A., Zimmermann, K., Ateia, M., et al., 2023. Application of Neural Network in Metal Adsorption Using Biomaterials (BMs): A Review. Environmental Science Advances. 2, 11–38. DOI: https://doi.org/10.1039/d2va00200k

[21] Fiyadh, S.S., Alardhi, S.M., Al Omar, M., et al., 2023. A Comprehensive Review on Modelling the Adsorption Process for Heavy Metal Removal From Wastewater Using Artificial Neural Network Technique. Heliyon. 9(4), e15455. DOI: https://doi.org/10.1016/j.heliyon.2023.e15455

[22] Bezerra, M.A., Santelli, R.E., Oliveira, E.P., et al., 2008. Response Surface Methodology (RSM) as a Tool for Optimization in Analytical Chemistry. Talanta. 76(5), 965–977. DOI: https://doi.org/10.1016/j.talanta.2008.05.019

[23] Rezaeinia, S., Ebrahimi, A.A., Dalvand, A., et al., 2023. Application of Artificial Neural Network and Dynamic Adsorption Models to Predict Humic Substances Extraction From Municipal Solid Waste Leachate. Scientific Reports. 13, 12421. DOI: https://doi.org/10.1038/s41598-023-39373-2

[24] Haykin, S., 2009. Neural Networks and Learning Machines, 3rd ed. Pearson Education: Upper Saddle River, NJ, USA.

[25] Afolabi, F.O., Musonge, P., Bakare, B.F., 2021. Bio-Sorption of Copper and Lead Ions in Single and Binary Systems Onto Banana Peels. Cogent Engineering. 8(1), 1886730. DOI: https://doi.org/10.1080/23311916.2021.1886730

[26] Edet, U.A., Ifelebuegu, A.O., 2020. Kinetics, Isotherms, and Thermodynamic Modeling of the Adsorption of Phosphates From Model Wastewater Using Recycled Brick Waste. Processes. 8(6), 665. DOI: https://doi.org/10.3390/pr8060665

[27] Foo, K.Y., Hameed, B.H., 2010. Insights Into the Modeling of Adsorption Isotherm Systems. Chemical Engineering Journal. 156(1), 2–10. DOI: https://doi.org/10.1016/j.cej.2009.09.013

[28] Chand, P., Bafana, A., Pakade, Y.B., 2015. Xanthate Modified Apple Pomace as an Adsorbent for Removal of Cd (II), Ni (II) and Pb (II), and Its Application to Real Industrial Wastewater. International Biodeterioration & Biodegradation. 97, 60–66. DOI: https://doi.org/10.1016/j.ibiod.2014.10.015

[29] Gomravi, Y., Karimi, A., Azimi, H., 2021. Adsorption of Heavy Metal Ions via Apple Waste Low-Cost Adsorbent: Characterization and Performance. Korean Journal of Chemical Engineering. 38(9), 1843–1858. DOI: https://doi.org/10.1007/s11814-021-0802-8